Astron. Astrophys. 334, 953–968 (1998)

ASTRONOMY
AND
ASTROPHYSICS

# Full spectrum of turbulence convective mixing: I. theoretical main sequences and turn-off for 0.6 ÷ 15 $M_\odot$

**Paolo Ventura**[1], **Anna Zeppieri**[2], **Italo Mazzitelli**[1] **and Francesca D'Antona**[3]

[1] Istituto di Astrofisica Spaziale C.N.R., Via del Fosso del Cavaliere, I-00133 Roma, Italy
[2] Collegio Leoniano, Anagni, Italy
[3] Osservatorio Astronomico di Roma, I-00040 Monteporzio, Italy

Received 12 December 1997 / Accepted 6 March 1998

**Abstract.** We present the results of extensive evolutionary computations from the Zero Age Main Sequence to the Red Giants, for stars in the range $0.6 \div 15 M_\odot$ and with chemistry ($Y$, $Z$) = (0.274, 0.017). The novelty of these computations is in the general treatment of convection, namely:

1. convection as a whole is addressed in the Full Spectrum of Turbulence model (billions of eddy scales are considered) with the appropriate convective fluxes distribution, as opposed to the one-eddy Mixing Length Theory;

2. local chemical evolution also in the presence of convection is separately evaluated for each element, as a result of a process in which nuclear evolution and turbulent transport are fully coupled by means of a diffusive scheme (coupled-diffusion);

3. convective overshooting (when considered) is also addressed in the above coupled-diffusive scheme, assuming that the turbulent velocity exponentially vanishes outside the formally convective region according to an e-folding free parameter $\zeta$, tuned to fit observations.

After some tests on the small solar convective core in early main sequence, we discuss the effects of coupled-diffusion in the cores of larger mass stars, where the nuclear lifetimes of some (p–p and) CNO elements can be comparable to the mixing times. We also compute a full grid of tracks with a small amount of overshooting, finding that *a unique free parameter can be suitable for the whole range of mass considered (solar and below solar included)*. Theoretical tracks are discussed, and isochrones are compared to the observational HR diagram for the Pleiades, finding an age $\gtrsim$ 120 Myr, consistent with that obtained from the candidate brown dwarf PPL 15. An age is also derived for the young cluster $\alpha$ Persei, for which a datation from the detection of lithium in brown dwarf candidates should be soon available. For completeness, and to facilitate comparisons with results by other authors, we also describe in details the **ATON 2.0** code used for the present computations.

**Key words:** stars: evolution of – convection – numerical methods

## 1. Introduction

In the vast majority of the stellar evolutionary computations up today, turbulent convection has been described as a *local* mechanism (in spite of its intrinsic *non-local* character) according to the Mixing Length Theory (MLT). In the local approximation, at the Schwarzschild boundary both velocity and acceleration go to zero together with the buoyancy forces acting on the convective elements, and nothing can be known about the turbulent velocity profiles outside formally convective regions. In addition, in convective and overshooting regions instantaneous chemical mixing decoupled from nuclear evolution is generally assumed in stellar modeling, with the only noticeable exception of Sackmann et al. (1995) for the external layers of Asymptotic Giant Branch (AGB) stars, where coupling nuclear evolution and mixing is the only correct way of describing the surface lithium evolution.

And yet, both overshooting and chemical evolution in turbulent regions do affect the behavior of stars. Let us first consider overshooting alone. Some attempts have been made to predict – very often according to *non-local* corrections to the MLT – the amount of mixed matter (Shaviv & Salpeter 1973; Roxburgh 1978, Xiong 1985, Grossman 1996 etc.); many such models have been reviewd and criticized on theoretical grounds by Canuto (1992, 1996). When constructing stellar models, all the above approaches predict large overshooting distances ($\sim 1.4 \div 1.8 H_p$, being $H_p$ the pressure scale heigth) which should lead to dramatic – and not observed – consequences at least on the evolution of massive stars in young open clusters (Maeder 1990).

Computations with a bare parametric approach to the problem have been then also tried, allowing instantaneous mixing beyond the formal convective borders up to a fraction of $H_p$ (e.g. Maeder & Meynet 1987; Stothers & Chin 1992). According to Maeder & Meynet (1991), the main sequences of young clusters are reasonably fit with an instantaneous overshooting from the convective core $l_{ov} \sim 0.25 H_p$; for older clusters (Turn Off (TO) masses $< 1.6 M_\odot$) the temporal evolution of the convective cores is more tricky, depending on details of the chemical and physical inputs (Maeder & Meynet 1987). An analogous

*Send offprint requests to*: I. Mazzitelli

upper value to overshooting ($l_{ov} \sim 0.20 H_p$) has been also suggested by Stothers & Chin (1992).

As for *non-instantaneous* mixing (and overshooting), Deng et al. (1996a,b, always in an MLT framework) suggested that it is more physically realistic to expect smooth chemical profiles outside the convective boundaries, consistent with a diffusive description of the process. In the present paper we adopt a diffusive approach too, with considerable conceptual differences with respect to all the previous studies to be discussed in details in the following.

As for the effects of coupling nuclear evolution to non-instantaneous mixing, we only found sparse references in the literature to the problem as a whole, and to possible rough solutions with complete mixing if nuclear lifetimes are longer than mixing times, locally frozen compositions in the opposite case. In the best of our knowledge, the present computations are the first ones in which the problem has been consistently and extensively addressed, apart from the already quoted case by Sackmann et al. (1995) in AGB. Full Spectrum of Turbulence (FST) convection model, and coupling between nuclear evolution and diffusive mixing, are then the main differences between the present paper and all the preceding literature.

## 2. The convective model

### *2.1. Convection as a whole*

A short discussion on the convective model adopted in the present computations is unavoidable, since the results obtained with diffusive mixing depend on the convective velocities and scale lengths.

Convection in stars is by far turbulent, the largest eddies having a size comparable to that of the entire convective region ($\sim 10^9 \div 10^{12}$ cm). They break down pumping (downscatter) and getting back (backscatter) kinetic energy into smaller eddies, until molecular viscosity takes over, and the kinetic energy stored in the whirlpools is thermally dissipated; billions of eddy scales are then present in stars. Navier–Stokes equations describing this process from first principles are both non-linear and non-local (Xiong 1985, Canuto 1992, Grossman 1996), and their analytical or numerical solution for a general stellar case is not yet available. In stellar modeling, we then still stick to *local* models to compute both the energy fluxes and the convective scale lengths.

As for the fluxes, MLT (Prandtl 1925) – originally developped for very viscous fluids – was first applied by Vitense (1953) to stellar modeling. In the MLT, the spectral distribution of eddies is mimicked by one "average" eddy only. More updated models provide now fluxes also for low-viscosity flows, in which the whole eddy spectrum is accounted for (Canuto & Mazzitelli 1991 and 1992, Canuto et al. 1996–CGM). Stothers & Chin (1995) defined Full Spectrum of Turbulence (FST) these latter models, as opposed to the one-eddy spectrum MLT. In the present work we adopt the FST scheme with the CGM fluxes.

The scale length $\Lambda$ was originally chosen, in the MLT, coincident with the distance $z$ from the convective boundary, consistently with Von Karman law for incompressible fluids (Prandtl 1925). Since however the one-eddy flux distribution is very crude, no realistic fit of the Sun could be obtained. It is then now customary to apply the MLT with $\Lambda = \alpha H_p$, where $\alpha$ is a free parameter tuned on the solar model; depending on the micro-physical inputs, $1.5 \leq \alpha \leq 2.2$.

The more physically correct choice $\Lambda = z$ close to the convective boundaries is instead allowed in an FST framework. However, far from the boundaries, also $\Lambda$ must, in a star, approach the hydrostatic scale length $H_p$. To match these requirements, we consider both the upper and the lower convective boundary; we compute for each convective grid point $z^{up}$ and $z_{low}$ and assume $z$ as their harmonic average. Close to the boundaries $z \simeq z^{up}$ or $\simeq z_{low}$, which is the required result. For deeper layers, let us recall that, in a polytropic structure of index $n$, $z \approx (1+n)H_p$ (Lamb 1932). In convective regions $n \sim 1.5$, that is: $z \sim 2.5 \cdot H_p$. The harmonic average gives $z \equiv z^{up}/2 \equiv z_{low}/2 \sim 1.25 \cdot H_p$, again close to the required value.

No *perfect* theory of convection, however, still exists, and the same is true for all other micro/macro-physical inputs. If we then ask for an *exact* fit of the Sun, some tuning of the models is required. With the MLT, *all* the physical uncertainties are usually reset by means of the *completely* free parameter $\alpha$. At variance, in an FST environment we recall that $\Lambda$ should also allow for overshooting ($\Lambda = z + OV$), which is not yet known from first principles. We can then parametrize $OV = \beta H_p^{top}$ (or $OV = \beta H_p^{bot}$), such that $\beta$ can be seen as a *fine tuning parameter*, constrained by $0 \leq \beta \leq 0.25$ (Maeder & Meynet 1991, Stothers & Chin 1992). Note that FST tuning affects only layers close to the boundaries since, for inner layers, $z$ fastly grows $\gg OV$. With CGM fluxes (Kolmogorov constant updated to $Ko = 1.7$) the solar fit requires $\beta \sim 0.1$, the value slightly depending on the chemical abundance chosen. With $OV = 0$ one would get an underestimate of the solar $T_{\rm eff}$ around 1.5%; too much for helioseismological purposes, but almost negligible in the more general framework of stellar evolution. In the present paper we will always adopt

$$\Lambda = z^{up} \cdot z_{low}/(z^{up} + z_{low})$$

unless differently specified, where $z^{up}$ is the distance from the top of convection increased by $\beta H_p^{top}$, and analogously for $z_{low}$.

### *2.2. Diffusive mixing and overshooting*

According to first principles, in the presence of both nuclear reactions and turbulent mixing, the local temporal variation of the $i^{th}$ element follows the diffusion equation (Cloutman & Eoll 1976):

$$\left(\frac{dX_i}{dt}\right) = \left(\frac{\partial X_i}{\partial t}\right)_{nucl} + \frac{\partial}{\partial m_r}\left[(4\pi r^2 \rho)^2 D \frac{\partial X_i}{\partial m_r}\right]. \qquad (1)$$

stating mass conservation of element $i$ if molecular diffusion be negligible with respect to turbulent diffusion (almost always true). The diffusion coefficient D is:

$$D = 16\pi^2 r^4 \rho^2 \tau^{-1} \qquad (2)$$

where $\tau$, the turbulent diffusion timescale, is related to the one-point density-radial velocity correlation

$$< \rho_i' u' >= -\tau \partial \rho_i / \partial r \quad (3)$$

Unfortunately, knowledge of the second order momentum in Eq. (3) requires previous solution of the Navier-Stokes Eqs. for a compressible stellar fluid, not yet available in the huge variety of cases of astrophysical interest. Also for $D$ a local approximation is then customarily used, that is: $D = u l_d/3$, where $u$ is the average turbulent velocity and $l_d$ ($= \Lambda$ in the formally convective region) is the convective scale length.

In an MLT framework, the above approximation is highly disputable since experiments show that turbulent chemical mixing is more efficient at the *smallest* scales, at variance with the unique (*largest*) MLT scale. More physically sound is the FST description: the average velocity accounts also for the smallest eddies, and the scale length is always the more correct one. In our case we then expect to get a better approximation to the "true" diffusion coefficient.

Turbulent velocity $u$ is computed according to Eqs. (88), (89) and (90) by CGM. One problem arises because of the "locality" of the FST model ($u$ at the convective boundaries vanishes). However, $u$ sharply goes to zero only very close to the boundaries; a little deeper in the convective region, the velocity profile approaches to a plateau. It is then possible to extrapolate a "reasonable" non-vanishing velocity at the formal boundary, and test computations starting from a pressure either 2%, 5% or 10% inside the boundary gave almost identical results. We then extrapolate $\log u$ vs. $\log P$ to get the turbulent velocity at the formal boundary starting from a pressure 5% inside.

As for diffusive overshooting (if any) we recall that, according to Xiong (1985), turbulent velocity exponentially vanishes outside formally convective regions. We then write, in overshooting regions:

$$u = u_b \exp \pm \left( \frac{1}{\zeta f_{thick}} \ln \frac{P}{P_b} \right) \quad (4)$$

where $u_b$ and $P_b$ are respectively turbulent velocity and pressure at the convective boundary, $P$ is the local pressure, $\zeta$ is a free parameter to be tuned as discussed in the following, and $f_{thick}$ is the thickness of the convective region in fractions of $H_p$ (maximum value of $f_{thick} = 1$), to maintain a non-locality flavor, since $f_{thick}$ scales overshooting according to the thickness of the convective region. While the diffusive scale length in formally convective regions is obviously $l_d = \Lambda$ as in Sect. 2.1, in the overshooting regions we use $l_d = \beta H_p$ to maintain continuity of the diffusive coefficient D at the boundaries.

In a first approximation, then, our framework for diffusive mixing and overshooting shows similarities to the one by Deng et al. (1996a,b). However:

a) use of FST instead of MLT, with different diffusive velocities and scale lengths, leads to different results, and:

b) the chemical evolutionary scheme is far different in our case, since we fully couple nuclear evolution and diffusive mixing (hereafter to: "coupled-diffusion").

Of course, **ATON 2.0** code also allows computations with instantaneous mixing and overshooting (in this latter case, the overshooting distance is simply $\nu H_p$ as usual). In the following, comparisons between results obtained with instantaneous mixing and coupled-diffusion will be presented.

### *2.3. Coupled mixing and nuclear evolution*

When using Eq. (1) two alternatives choices could be made:

a) numerically evaluate $(\partial X_i/\partial t)_{nucl}$ as a function of local abundances and cross sections, substitute in Eq. (1) and only then apply the diffusive algorithm. The bonus of this choice is that the problem is reduced to a "semi-local" one: no large matrices must be stored and computations are relatively fast. The drawback is that nuclear evolution is completely decoupled from mixing, and some mechanisms –like hot bottom burning lithium production in the envelopes of AGB stars (Sackmann et al. 1995), or effect of mixing on the CNO equilibria – cannot even be addressed;

b) analytically expand $(\partial X_i/\partial t)_{nucl}$ as a function of local abundances and cross sections, and solve it together with the diffusion matrix for the whole stellar structure. If $chem$ is the number of chemical species and $grid$ is the number of grid points, a matrix of rank $(chem \cdot grid) \times (chem \cdot grid)$ – typically $100 \div 500$ MB – must be stored and inverted. Method b) severely threatens any workstation, but correctly couples nuclear evolution to the contemporary change of composition due to turbulent transport of matter (coupled-diffusion).

We then made choice b) which, after some algebraic manipulations fully described in Sect 9.4, can be reduced to the storage and inversion of a matrix of rank $(3 \cdot chem) \times (chem \cdot grid)$ – typically $\sim 1 \div 3$ MB – well affordable according to safe and fast algorithms. For more details on the nuclear evolutionary scheme as a whole, see Sect. 9.3.

## 3. Micro-physical inputs

Since comparisons with former results by different authors will turn out somehow elusive due to our previously untested evolution/convection/mixing combination, we felt obliged to at least summarize and shortly describe the micro-physical inputs in **ATON 2.0**. In the Appendix, also the main numerical features of the code will be addressed.

### *3.1. Thermodynamics*

Thermodynamics tables are given as a function of temperature and pressure. In **ATON 2.0** they are built, for any given metal abundance $Z$, in three steps.

First, the tables by Magni & Mazzitelli (MM 1979, recently updated in full ionization regime) are stored for the five $H$–abundances: $X = 1.0 - Z$; $X = .8 - Z$; $X = .5 - Z$; $X = .2 - Z$; $X = 0.0$. Since MM tables were computed for $Z = 0$, an "average" metal is interpolated from the pure-carbon table by Graboske et al. (1973). This latter procedure satisfactorily mimicks an EOS with metals at least as long as $Z \leq Z_\odot$. A

former release of MM EOS has been however shown by Saumon (1994) somewhat biased in high-T, low–$\rho$ regions, while the $P = P(\rho, T)$ relation performs fairly well in the low-T, high–$\rho$ non-ideal gas regime.

A severe warning is here necessary: contrarily to some more recent EOS' for non-ideal gas (e.g. Saumon et al. 1995), MM thermodynamics has been computed not only for *pure* $H$ or $He$ chemical compositions, but also for $H/He$ *mixtures*. In spite of its age, it is then still more physically updated than other EOS' in pressure dissociation and ionization domain, where interpolation (with the additive volumes law or any other such scheme) between *pure* elements is bound to give unreliable results, due to the *physical* influence of $H$-ions on the $He$-bound states.

As a second step, the tables (covering the $\rho$-T plane up to densities where the lattice ion quantum effects begin to show up) are partially overwritten by the Mihalas et al. (MHD, 1988) equation of state, for the chosen Z and in the range Log $T \leq 5$; Log $\rho \leq -2$. MHD EOS is in fact biased (Saumon 1994) at larger densities, where the MM EOS is instead still quite good. With this second step, correct allowance for $Z$ is obtained in the low-T, nearly ideal gas region, but for the unique $H/He$ ratio for which the MHD EOS are provided.

Third and final step: the above tables are partially overwritten by the OPAL EOS tables (Rogers et al. 1996) where available ($3.7 \leq LogT \leq 8.7$), for the same five $H/He$ ratios as in MM. In this way, residual anomalies (if any) at high-T in the MM EOS are forgotten, and variable $H/He$ ratios are restored in all the cases of interest.

Lastly, one pure-carbon and one pure-oxygen table, computed in full ionization regime with an improved MM-like scheme, are addedd. Bicubic logaritmic interpolation on both P and T are performed on the tables at fixed H-abundances, and linear interpolation on the chemical composition follows, to evaluate the various thermodynamical quantities.

### 3.2. Opacity

A procedure similar to the above one is performed also for the opacities. For each given $Z$, OPAL opacities (Rogers & Iglesias 1993), linearly extrapolated ($\log \kappa$ vs. $\log \rho$) in the high–$\rho$ region, and harmonically added to conductive opacities (Itoh & Kohyama, 1993), form the ground level.

At lower temperatures ($T < 6000$K), Alexander & Ferguson's (1994) molecular opacities (plus electron conduction when in full ionization) complete the tables, for the same 10 $H/He$ ratios as in OPAL's case. At variance, Kurucz (1993) low temperatures ($T < 6000$K) opacities can be used, but for one $H/He$ ratio only.

For $He/C/O$ mixtures, interpolation on fifteen out of the 60 OPAL tables (plus conductive opacities) is performed. Comparisons with the full set of 60 tables show that, with the present reduced set, interpolation on the chemical composition always gives agreement better than $2\%$ and, in the vast majority of cases, better than $1\%$. Bicubic logaritmic interpolation on both $\rho$ and $T$ are performed on the tables at a fixed $H/He$ ratio, and quadratic interpolation on $H$ follows to get the final opacity value.

### 3.3. Nuclear network

It includes the 14 elements: $^1H$, $^2H$, $^3He$, $^4He$, $^7Li$, $^7Be$, $^{12}C$, $^{13}C$, $^{14}N$, $^{15}N$, $^{16}O$, $^{17}O$, $^{18}O$, $^{22}Ne$. We explicitly consider the following 22 reactions:

$$
\begin{array}{l}
p + p \longrightarrow^2 H + e^+ + \nu \\
p + p + e^- \longrightarrow^2 H + \nu \\
^2H + p \longrightarrow^3 He + \gamma \\
^3He +^4 He \longrightarrow \alpha + 2p \\
^3He +^4 He \longrightarrow^7 Be + \gamma \\
^7Li + p \longrightarrow 2\alpha \\
^7Be + p \quad (\longrightarrow^8 B + \gamma \longrightarrow^8 Be) \longrightarrow 2\alpha \\
^7Be + e^- \longrightarrow^7 Li + \gamma \\
^{12}C + p \quad (\longrightarrow^{13} N + \gamma) \longrightarrow^{13} C + e^+ + \nu \\
^{13}C + p \longrightarrow^{14} N + \gamma \\
^{14}N + p \quad (\longrightarrow^{15} O + \gamma) \longrightarrow^{15} N + e^+ + \nu \\
^{15}N + p \longrightarrow \alpha +^{12} C \\
^{15}N + p \longrightarrow^{16} O + \gamma \\
^{16}O + p \quad (\longrightarrow^{17} F + \gamma) \longrightarrow^{17} O + e^+ + \nu \\
^{17}O + p \longrightarrow \alpha +^{14} N \\
^{17}O + p \quad (\longrightarrow^{18} F + \gamma) \longrightarrow^{18} O + e^+ + \nu \\
^{18}O + p \longrightarrow^{15} N + \alpha \\
3\alpha \rightarrow^{12} C + \gamma \\
^{12}C + \alpha \rightarrow^{16} O + \gamma \\
^{14}N + \alpha (\rightarrow^{18} F + \gamma) \longrightarrow^{18} O + e^+ + \nu \\
^{12}C +^{12} C \rightarrow \alpha/2 +^{22} Ne \\
^{18}O + \alpha \rightarrow^{22} Ne + \gamma
\end{array}
$$

The reactions in parentheses are so fast that they are not explicitated (in terms of mixing, the half-lifes of the elements are so short that they are always in *local* equilibrium). The cross sections for the other reactions are from Caughlan & Fowler (1988); low, intermediate and strong screening coefficients are from Graboske et al. (1973). The $^{12}C +^{12} C$ reaction has been given a fictitious end in $\alpha/2 +^{22} Ne$, since **ATON 2.0** code can follow $^{12}C$-ignition, but has not been set to deal with more advanced evolutionary phases.

Logaritmic nuclear cross sections are in tables with a very thin spacing in Log $T$, and are cubically interpolated.

### 3.4. Neutrinos

Pair, photo, bremsstrahlung and plasma neutrino have been taken from Itoh et al. (1992). Recombination neutrinos have not been included, since they are of interest only for more advanced (pre-supernova) evolutionary phases, which presently lie out of the domain of **ATON 2.0**.

Due to the computing time required to evaluate the various neutrino fluxes with the fitting formulae in the literature, we built up logaritmic tables of neutrino rates for various elements. Bicubic logaritmic interpolation on both $\rho$ and $T$ are performed on the tables at a fixed chemistry, and linear interpolation on the chemistry follows to compute the neutrino emission.

### 3.5. $^4He$ sedimentation

Also gravitational settling and chemical and thermal diffusion of $^4He$ is optionally included in **ATON 2.0**. To avoid confusion with the term *diffusion*, for which we prefer to maintain the meaning of *mixing due to turbulent convection*, in the future, we will refer to all the processes leading to $^4He$ settling as *sedimentation* tout court.

The following approximations are made, consistently with Muchmore (1984) and Paquette et al. (1986):

- radiative force can be neglected
- all particles, including the electrons, have approximately Maxwellian distribution
- mean thermal velocities are much larger than the diffusion velocities
- magnetic fields are absent.

The sedimentation velocities then satisfy (Proffitt & Michaud 1991; Paquette et al. 1986):

$$\frac{d\,p_a}{dt} - \frac{\rho_a}{\rho}\cdot\frac{d\,p}{dr} - n_a Z_a e E = \sum_j K_{aj}(w_a - w_j) + \frac{n_a n_j}{n_a + n_j}\alpha_T k \frac{d\,T}{dr} \quad (5)$$

where $p_a, \rho_a, n_a, Z_a, w_a$ are the partial pressure, mass density, number density, mean charge, and sedimentation velocity for species *a* (in our case, respectively: $^1H$, $^4He$ and electrons), and $E$ is the electric field induced by the gradients in ion densities (Aller & Chapman 1960). The resistance coefficients $K_{aj}$ are taken from a fit (Iben & Mc Donald 1985) of the numerical results by Fontaine & Michaud (1979), while for the total thermal diffusion we adopt $\alpha_T = 2.54Z_2^2 - .804Z_2$ (Alcock & Illarianov 1980).

In terms of temperature gradient and number density, Eq. (5) may be rewritten as:

$$\frac{1}{n_a}\sum_j K_{aj}(w_a - w_j) - Z_a e E = -A_a m_H g - kT\frac{d\,\ln T}{dr} + \alpha_T \frac{n_j}{n_a + n_j} k \frac{d\,T}{dr} - kT\frac{d\,\ln n_a}{dr}$$

where $A_a$ is the molecular weight for the $a^{th}$ species, while $m_H$ is the hydrogen mass.

To complete the set of equations we apply the condition for no net mass flow relative to the center of mass and no electrical current. To proceed, we separate out the velocity therm $w_a$ as:

$$w_a = w_a^{gt} - \sum_j \sigma_{aj}\frac{d\,\ln n_j}{dr}\,,$$

where $w_a^{gt}$ is relative to the gravity components and temperature gradient, while the summatory is relative to the components due to gradients in number densities, that is:

$$w_1^{gt} = \frac{G+H}{D}\;;\; w_2^{gt} = -\frac{G+H}{D}\cdot\frac{\alpha_1}{\alpha_2}$$

where all the symbols have the same meaning as in Iben & McDonald (1985) but for $H$ (due to thermal diffusion, not present there):

$$H = \alpha_2\left[(n_2\beta_1 - n_1\beta_2) - \alpha_T\cdot\frac{n_1 n_2}{n_1+n_2}(\beta_1 - \beta_2)\right]k\frac{dT}{dr}\,.$$

We then use these expressions in the continuity equation:

$$\frac{\partial\, n_a}{\partial t} = -\frac{1}{r^2}\frac{\partial}{\partial r}\left[r^2\left(w_a^{gt} - \sum_j \sigma_{aj}\frac{d\,\ln n_j}{dr}\right)\right]$$

which can be solved by a conservative, semi-implicit finite difference method of first-order in time and second-order in the spatial variable $r$, always following the procedure by Iben & Mc Donald (1985).

## 4. The solar model

### 4.1. The early convective core

We first computed a bunch solar evolutionary tracks with metal abundances $Z = 0.017$ and $Z = 0.020$, bracketing the actual value of $Z_\odot$ (Grevesse 1984; Grevesse & Noels 1993). We started from homogeneous main sequence and followed evolution up to an age of $\sim 5$ Gyr, slightly larger than the presently accepted solar age of $4.6 \pm 0.1$ Gyr. Pre-main sequence phases with deuterium burning were not accounted for; so we started the computations with no $^3He$. The initial $^4He$ abundance $Y_0$ was adjusted for each track to fit the observed solar luminosity, and the fit of the observed radius was achieved by fine tuning of the FST parameter $\beta$.

In all, 20 tracks were computed as detailed in Table (1). In all the $\nu > 0$ cases, instantaneous mixing and overshooting ($\Lambda_{ov} = \nu H_p$) were present; when $\zeta > 0$ coupled-diffusion plus overshooting (Eq. (4)) were adopted. The $\nu = \zeta = 0$ case can be seen as representative of both instantaneous mixing and/or coupled-diffusion, since for the small solar convective core in early main sequence both treatments give almost exactly the same results. For larger mass stars, when CNO burning in convective core dominates the structure, the case is different as we will see later on.

Some of the main results are shown in Table (2), where also the thickness of the external convective envelope (in fractions of the solar radius) and the present surface helium abundance (when sedimentation is active) are reported. Note en passant that models with Z=0.020 and sedimentation seem to better fit the helioseismologically "observed" thickness of the convective envelope $R_{conv} = .287 \pm .003 R_\odot$ (Christensen–Dalsgaard et al. 1991). Conclusions about the solar metal abundance from these data would be however premature, since any further small revision of radiative opacities, or even an overshooting from the bottom of convection by a few thousand Km (smaller than the upper limit of $\sim 0.05 H_p$ suggested by Basu & Antia, 1997) could still change the picture.

For completeness, we also show in Table 3 the neutrino fluxes in SNU predicted for all the solar models computed.

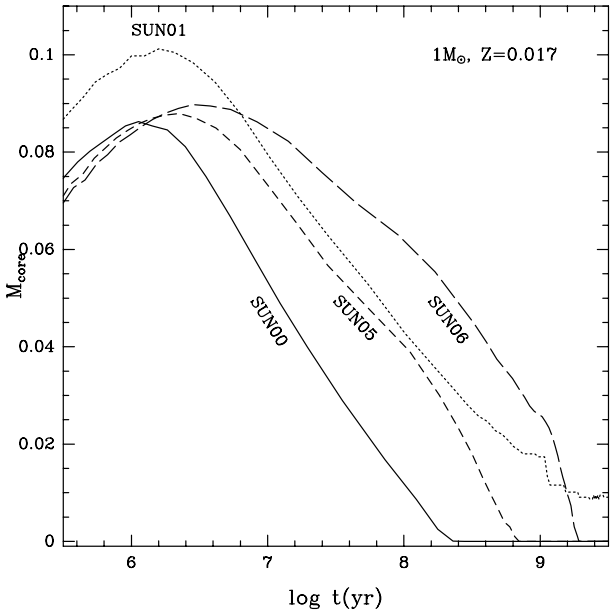


**Fig. 1.** Evolution of the initial solar convective core versus time, for various choiches of the $\zeta$ (diffusive overshooting) or $\nu$ (instantaneous overshooting) parameter. The larger is the extra-mixing, the longer the duration of the convective core

**Table 1.** Legend of the labels for the evolutionary sequences computed. For the ten choices of convection modeling and diffusion displayed with the last digit, the two choices of metallicities are displayed by the penultimate digit

| Track | $\nu_{inst.ov.}$ | $\zeta_{diff.ov.}$ | *sed.* |
|---|---|---|---|
| SUNX0 | 0.0 | 0.000 | NO |
| SUNX1 | 0.05 | 0.000 | NO |
| SUNX2 | 0.1 | 0.000 | NO |
| SUNX3 | 0.2 | 0.000 | NO |
| SUNX4 | 0.0 | 0.010 | NO |
| SUNX5 | 0.0 | 0.020 | NO |
| SUNX6 | 0.0 | 0.040 | NO |
| SUNX7 | 0.0 | 0.010 | YES |
| SUNX8 | 0.0 | 0.020 | YES |
| SUNX9 | 0.0 | 0.040 | YES |
| SUN0Y Z=0.017 | | | |
| SUN1Y Z=0.020 | | | |

Our results are largely consistent with those by Bahcall & Pinsonneault (1992), both with and without helium sedimentation. Overshooting, even if slightly changing the central $^3He$ abundances as discussed in the following, does not substantially modify the $^7Be$ fluxes, also because the more than 80% of the solar $^3He$ is consumed via the $^3He +^3 He$ channel.

Let us now discuss the behavior of the small, early solar convective core, as depicted in Fig. 1 for the Z=0.017 case (the Z=0.020 case shows only small quantitative differences). Even if the argument is not a strict novelty, it will help to elucidate the qualitative differences between instantaneous and diffusive overshooting.

**Table 2.** Thickness of the convective envelope and $^4He$ abundance at the surface of the models computed. The second and fifth columns give the initial $^4He$ abundance adopted to fit the present solar luminosity

| Model | $Y_0$ | $R_c \setminus R_\odot$ | $Y_s$ | Model | $Y_0$ | $R_c \setminus R_\odot$ | $Y_s$ |
|---|---|---|---|---|---|---|---|
| SUN00 | 0.269 | 0.273 | | SUN10 | 0.282 | 0.280 | |
| SUN01 | 0.270 | 0.275 | | SUN11 | 0.282 | 0.285 | |
| SUN02 | 0.270 | 0.278 | | SUN12 | 0.282 | 0.288 | |
| SUN03 | 0.272 | 0.287 | | SUN13 | 0.284 | 0.296 | |
| SUN04 | 0.269 | 0.274 | | SUN14 | 0.282 | 0.280 | |
| SUN05 | 0.269 | 0.274 | | SUN15 | 0.282 | 0.281 | |
| SUN06 | 0.269 | 0.274 | | SUN16 | 0.282 | 0.280 | |
| SUN07 | 0.271 | 0.277 | 0.2602 | SUN17 | 0.284 | 0.283 | 0.27313 |
| SUN08 | 0.271 | 0.276 | 0.2613 | SUN18 | 0.284 | 0.283 | 0.27435 |
| SUN09 | 0.271 | 0.276 | 0.2629 | SUN19 | 0.284 | 0.283 | 0.27595 |

At the beginning of ZAMS, when Log $T_c \sim 7.15$, the initial $^{12}C$ abundance is quite large ($^{12}C/Z \sim 0.18$), and transformation of $^{12}C$ into $^{14}N$ is responsible for the generation of $\sim 10\%$ of the total luminosity very close to the center ($\sigma(^{12}C + p) \propto T^{18}$, very stiff with $T$). The $L/r^2$ ratio (and the radiative gradient) is sufficiently large to keep alive a convective core. $^{12}C$ is then consumed and convection tends to die in $\sim 70 \div 80$ Myr (test computations with initial $^{12}C = 0$ do not show a very early convective core).

In the meantime, $^3He$ begins to be produced; its equilibrium concentration reaches a maximum and, when $^{12}C$ is exhausted and $T_c$ increases to allow the $p-p$ chain to fully power the star, also central $^3He$ decreases. Since ($\sigma(^3He +^3 He) \propto T^{15}$, again quite stiff), a "large" abundance of $^3He$ could keep alive a convective core too. Actually, central conditions in the Sun (and also in stars of mass up to $\sim 1.2 M_\odot$) turn out such that, when the $p-p$ chain takes over, the central equilibrium concentration of $^3He$ is just slightly smaller than that required to maintain central convection. At this very point the presence of overshooting can play a role, as discussed in the next section.

### *4.2. Instantaneous vs. diffusive overshooting*

In general solar conditions, the lower is $T$, the larger the equilibrium abundance of $^3He$, which is then minimum at the center of the star and increases outwards, reaching a peak abundance around $\sim 0.3 \div 0.4 M_\odot$. Overshooting, then, mixes the core with surrounding matter overabundant in $^3He$ with respect to the central equilibrium concentration. This leads to overproduction of luminosity, maintaining large the radiative gradient and convection alive. $^{12}C$ is ineffective for this purpose since, once burned, is not produced any more. Figure 2 shows the small difference in $^3He$ abundance profiles with and without diffusive overshooting, sufficient to make the difference between an early death and a prolonged existence of a convective core.

**Table 3.** Computed neutrino fluxes. Results are expressed in Solar Neutrino Units (SNU)

| Model | $\phi(pp)$ $10^{10}$ | $\phi(pep)$ $10^{8}$ | $\phi(^7Be)$ $10^{9}$ | $\phi(^8B)$ $10^{6}$ | $\phi(^{13}N)$ $10^{8}$ | $\phi(^{15}O)$ $10^{8}$ | $\phi(^{17}F)$ $10^{6}$ |
|---|---|---|---|---|---|---|---|
| SUN00 | 6.060 | 1.380 | 4.080 | 4.364 | 3.298 | 2.672 | 3.205 |
| SUN01 | 6.081 | 1.384 | 4.130 | 4.550 | 3.332 | 2.679 | 3.222 |
| SUN02 | 6.085 | 1.383 | 4.331 | 4.708 | 3.542 | 2.887 | 3.525 |
| SUN03 | 6.072 | 1.356 | 4.473 | 3.630 | 3.698 | 3.067 | 3.785 |
| SUN04 | 6.064 | 1.382 | 4.106 | 4.425 | 3.329 | 2.704 | 3.244 |
| SUN05 | 6.065 | 1.382 | 4.104 | 4.426 | 3.325 | 2.699 | 3.245 |
| SUN06 | 6.059 | 1.379 | 4.089 | 4.463 | 3.330 | 2.701 | 3.253 |
| SUN07 | 6.074 | 1.378 | 3.982 | 4.180 | 3.105 | 2.497 | 2.983 |
| SUN08 | 6.075 | 1.379 | 3.984 | 4.185 | 3.105 | 2.497 | 2.985 |
| SUN09 | 6.075 | 1.379 | 4.008 | 4.306 | 3.152 | 2.544 | 3.052 |
| SUN10 | 5.992 | 1.348 | 4.534 | 5.485 | 4.558 | 3.825 | 4.674 |
| SUN11 | 5.977 | 1.342 | 4.600 | 5.800 | 4.660 | 3.924 | 4.834 |
| SUN12 | 5.996 | 1.347 | 4.880 | 5.954 | 4.967 | 4.212 | 5.259 |
| SUN13 | 5.977 | 1.320 | 5.050 | 4.780 | 5.190 | 4.466 | 5.641 |
| SUN14 | 5.994 | 1.348 | 4.540 | 5.498 | 4.563 | 3.830 | 4.683 |
| SUN15 | 5.997 | 1.349 | 4.559 | 5.553 | 4.591 | 3.858 | 4.724 |
| SUN16 | 5.992 | 1.348 | 4.553 | 5.612 | 4.605 | 3.869 | 4.747 |
| SUN17 | 6.008 | 1.347 | 4.4314 | 5.252 | 4.268 | 3.560 | 4.333 |
| SUN18 | 6.007 | 1.347 | 4.447 | 5.270 | 4.264 | 3.555 | 4.330 |
| SUN19 | 6.007 | 1.347 | 4.449 | 5.366 | 4.311 | 3.604 | 4.401 |

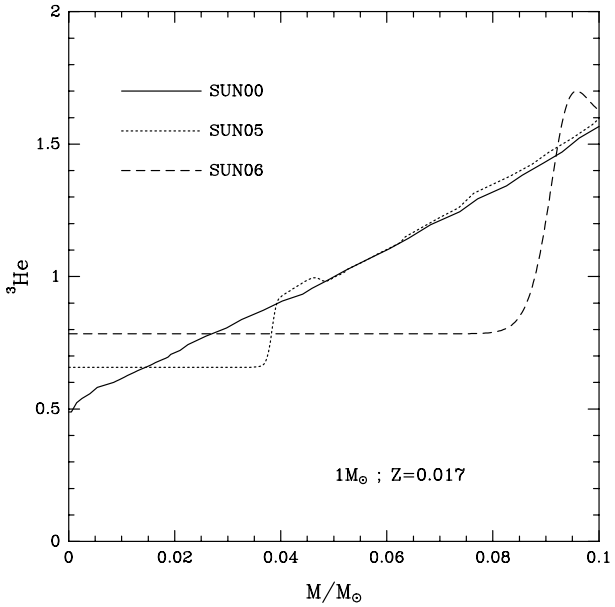


**Fig. 2.** The $^3He$ abundance profile (in units of $10^{-4}$) in the central part of the star at $\sim 2 \times 10^8$ yrs, without overshooting (solid line) and with two different values of the diffusive overshooting parameter $\zeta = 0.020$ (dotted line) and $\zeta = 0.040$ (dashed line). The larger the mixed region, the larger is also the central $^3He$ abundance, with prolongued life of the convective core

Let us finally discuss the different behaviors of the convective core with either instantaneous or diffusive overshooting. In the former case, the mixing boundary is plainly shifted outwards. According to the present results, instantaneous overshooting of $\sim 0.10H_p$ would suffice to give a steady convective core for the Sun until $H$-exhaustion and, in turn, to a detectable gap at the Turn-Off of old open clusters. Consistently with Maeder & Meynet (1987), we conclude that an overshooting this large must be excluded for solar mass stars.

More tricky is the case of diffusive overshooting, where mixing is a somewhat slow process which is almost complete only close to the Schwarzschild boundary, exponentially vanishing at large distances. For the Sun, diffusion with $\zeta \sim 0.02$ is *roughly* similar to instantaneous mixing with $\nu \sim 0.05$ (Fig. 1). And yet, no strict *equivalence* can be established, since a detailed analysis of the numerical results shows that, with $\zeta \sim 0.02$, *partial* diffusive mixing reaches farther than $0.05H_p$ beyond the formal convective boundary.

This test gives an hint about the profound differences between the two parameters $\nu$ and $\zeta$: to get almost the same amount of mixed matter, the numerical value of the latter must be lower than that of the former. Moreover, in the solar case $f_{thick} \leq 0.25$. According to Eq. (4) it is then likely that, for more massive stars with large convective cores ($f_{thick} = 1$), instantaneous overshooting with $\nu \sim 0.2$ should be *almost equivalent* to diffusive overshooting with $\zeta \sim 0.02$ as long as the amount of mixed matter is concerned. We then conclude that:

a) with diffusive overshooting, $\zeta \sim 0.02$ is a conservative estimate which does not modify the overall framework of solar evolution (also thanks to the "non-local" flavor arising from $f_{thick}$);

b) the same value of $\zeta$ is expected to mimick, for large mass stars, an instantaneous overshooting around $0.2H_p$, which is a "reasonable" choice according to Maeder & Meynet (1991) and Stothers & Chin (1992),

In the next of this paper, we will then compute evolutionary tracks and isochrones not only with $\zeta = 0$, but also with $\zeta = 0.02$ and, in some cases, with $\nu = 0.2$. Comparisons among theoretical results and to observations will then help us deciding whether or not $\zeta = 0.02$ is a sensible choice.

## 5. Evolutionary tracks

In this section we will present and discuss evolutionary tracks for stars having chemical composition Y=0.274, Z=0.017 (the lower limit for the solar metal abundance) in the range $0.6 \div 15M_\odot$, with and without diffusive overshooting. Tracks and isochrones for other compositions, mass ranges, $\zeta$ values etc. can be made available upon request, since both the **ATON 2.0** and the isochrones codes are largely authomatized.

Let us first discuss the main differences in the evolution up to central $^{12}C+^{12}C$ ignition for a star of $15M_\odot$, if we allow for either instantaneous mixing decoupled from nuclear evolution, or for coupled-diffusion (with and without overshooting), since – in the best of our knowledge – results with coupled diffusion have never been compared to results with nuclearly uncoupled diffusion or instantaneous mixing in MS.

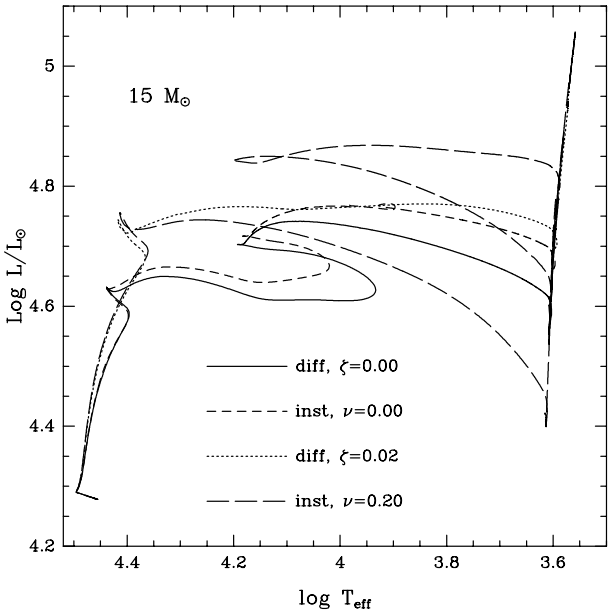


**Fig. 3.** HR diagram for a $15M_{\odot}$ star, when treating mixing and overshooting according to different schemes

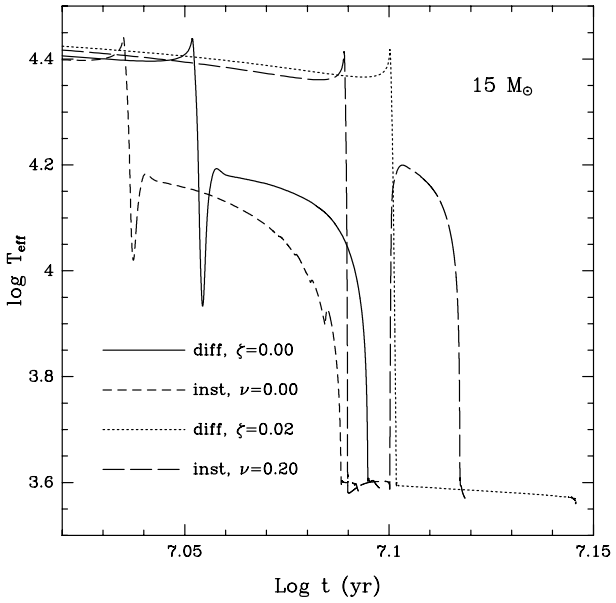


**Fig. 4.** Evolution of $T_{\rm eff}$ from the end of MS up to $^{12}C+^{12}C$ burning for a $15M_{\odot}$ star, when treating mixing and overshooting according to different schemes

### *5.1. Instantaneous mixing vs. coupled-diffusion*

In the case of instantaneous mixing, all the chemical abundances profiles are obviously flat in the convective core. Not so for coupled-diffusion. Let us focus our attention on this latter case, since it is by far the more interesting and physically sound one.

Among the nine CNO reactions explicitly accounted for (Sect. 3.3), the fastest one is by far $^{15}N+p \longrightarrow \alpha+^{12}C$; all the others have cross sections at least two orders of magnitude lower. The average nuclear lifetime of $^{15}N$ is $\tau(^{15}N)=\rho\sigma X_H$ where $\rho$ is the density, $\sigma$ the nuclear cross section of the reaction and $X_H$ the hydrogen abundance. This lifetime is to be compared to the turbulent diffusion time which, for the core of the $15M_{\odot}$ star in MS, is of the order of $10^5$s. For the p–p reactions (always contributing for less than 1% to the total luminosity), $^2D$ and $^7Li$ are the elements with shorter lifetimes.

At the beginning of MS, the central temperature ($\sim 30$ MK) is such that the lifetime of $^{15}N$ is still much larger than the mixing time; nearly complete mixing ensues both in the coupled-diffusive and in the instantaneous mixing case. $^2D$ and $^7Li$ lifetimes are instead short, and their central abundances are only a fraction of the abundances at the boundary of the convective core, but $p-p$ burning powers the star only for a minute fraction of the total. In the progress of evolution, however, $T_c$ increases up to $\sim 50\div 60$ MK; the lifetime of $^{15}N$ decreases and also the $^{15}N$ profile shows a minimum, of a few parts in ten thousands, at the centre of the star where the most of burning occurs.

Since H-burning is linear with each nuclear species involved (apart from the starting reaction of the p–p chain), central underabundances represent a bottleneck. The structure settles on a slightly lower luminosity than in the instantaneous mixing case, hardly detectable on Fig. 3 during the MS phase up to the overall contraction phase. The total duration on the MS phase is however somewhat increased. From Fig. 4, showing the behavior of $T_{\rm eff}$ vs. time in several mixing and overshooting cases, one can see that the total duration of MS is, with coupled-diffusion, about 4% longer than with instantaneous mixing. This is not any more a negligible difference in modern stellar modeling, since it is of the same order of magnitude of the differences presently found when updating the main micro-physical inputs like radiative opacities etc. Coupled-diffusion can not be omitted any longer in numerical computations of stellar evolution, if sound quantitative results are required.

After the overall contraction, the behaviors of the tracks with and without diffusion remain similar but not identical, due to the large sensitivity of the surface conditions on the $L_{3\alpha}/L_{Hshell}$ ratio, the larger being the ratio, the bluer appearing the star (central $3\alpha$ reactions ignite soon after central $H$-exhaustion). The delicate interplay among convective shells growing and merging around the convective core during MS and beyond (usually addressed to as *semiconvection*) is such that coupled-diffusion leads to slightly different chemical mixing and final chemistries in the region where the $H$-burning shell occurs, showing up amplified in the HR diagram.

This is not the place to address the long standing problem of the existence or not of the blue loop as a whole (see Chiosi 1997, and Salasnich et al. 1997 for a recent update). Suffice it to say the both our $15M_{\odot}$ models, with instantaneous mixing and coupled-diffusion, show this feature for the chosen chemistry, and none of them reaches the red supergiant region before the end of central $He$-burning. From Fig. 4, one can see that $C$-burning takes over as soon as the star reaches the Hayashi track. Even if we can not follow the details of $C$-burning with **ATON 2.0** code, we can in any case claim that the "red" phase for our $15M_{\odot}$ star lasts for less than 1% of its total lifetime, leading to

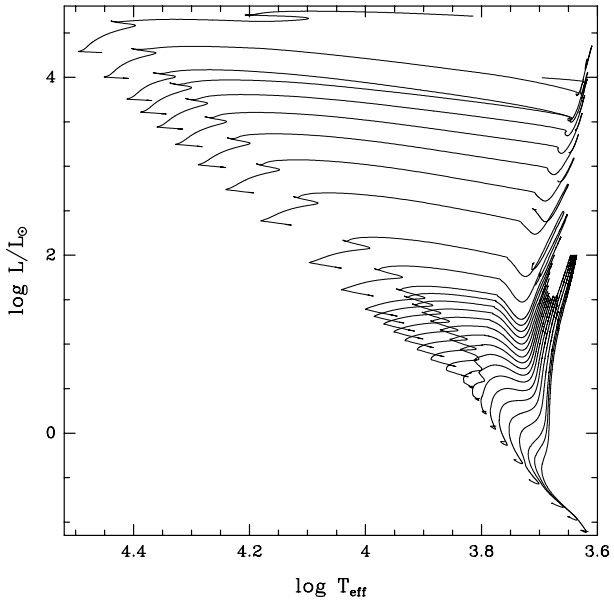


**Fig. 5.** HR diagram with no overshooting. The masses considered (in $M_{\odot}$) are: 0.6; 0.65; 0.7; 0.8; 0.9; 1.0; 1.1; 1.2; 1.3; 1.4; 1.5; 1.6; 1.7; 1.8; 1.9; 2.0; 2.1; 2.2; 2.5; 3; 4; 5; 6; 7; 8; 9; 10; 12 and 15

an expected deficiency of red supergiants of this mass. Different is the case if we include diffusive or instantaneous overshooting, as we will see right now.

### *5.2. Overshooting*

From Figs. 3 and 4 one can see that, for the $15M_{\odot}$ star, diffusive overshooting with $\zeta = 0.020$ is nearly equivalent to instantaneous overshooting with $\nu = 0.20$ as long as morphology and duration of MS is concerned. We will come back on the tuning of $\zeta$ when discussing the general results for the whole range of masses considered and the comparisons to the observations.

After the MS, in both cases the star reaches the Hayashi track at the beginning of the core $He$-burning phase. The main qualitative difference with the no-overshooting case – apart from the duration and the amplitude in the HR diagram of the MS – is that overshooting is included not only for the core convective region, but also for the surrounding convective shell, allowing these latter to mix in external regions, where no $H$-burning had yet modified the original $CNO$ abundances. As a result, at the end of MS, both $C$ and $N$ are now slightly overabundant in the H-burning shell than without overshooting, and the lower $L_{3\alpha}/L_{Hshell}$ ratio favors cooler surface conditions.

In the progress of time, however, the star with instantaneous overshooting goes back to the blue until core $He$-exhaustion and $C$-ignition. The star with diffusive overshooting, at variance with the above behavior, stays on the Hayashi track until $C$-ignition. The reason for this difference must be traced back in the presence of a convective region around the $H/He$ interface. The $H$-burning shell is thick enough that about $20 \div 30\%$ of the $H$-luminosity is born in the surrounding convective region.

With overshooting, the convective region is enriched in $CNO$ due to leakadge into more external regions, previously untouched by $H$-burning and, as above elucidated, the $H$-burning shell turns out more powered. However, with instantaneous overshooting, overabundance of $CN$ is present only once, at the beginning of the $H$-shell phase, and it is not refurbished by further and further overshooting; when $CN$ equilibrium is reached in the convective region, the shell is not overpowered any more, and the $L_{3\alpha}/L_{Hshell}$ ratio increases leading the star to the blue.

On the contrary, diffusive overshooting goes on penetrating the external layers slower than instantaneous overshooting, but for a larger extension – even if mixing there is only partial. Continuous enrichment of fresh $C$ and $N$ in the convective layer follows, and the efficiency of $H$-burning shell is kept larger (and almost constant) than with instantaneous overshooting. The ratio $L_{3\alpha}/L_{Hshell}$ always remains low enough to maintain the star in the red, and a blue loop never arises.

This different behavior leads to the prediction of a larger fraction of red supergiants ($11 \div 12\%$) in the diffusive case than in the instantaneous mixing one ($2 \div 3\%$). Careful comparisons (with adequate chemistry and statistics) between theoretical and observed star countings in MS and red supergiants for young open clusters, should be then a more powerful tool in tuning the value of $\zeta$ than thickness in the MS alone.

### *5.3. Tracks for smaller masses*

Let us now turn to the whole grid of models, from 0.6 to 15 $M_{\odot}$ in which diffusive overshooting has been included. For $1M_{\odot}$, as already seen (Fig. 1), $\zeta = 0.02$ leads to almost negligible effects. Figure 7 shows that the chosen amount of diffusive overshooting has almost no effect also upon the $1.1M_{\odot}$ star, while the $1.2M_{\odot}$ model begins to display a small remnant convective core at the TO, which it would not have shown without overshooting. For the chosen chemical composition, in fact, only the $1.3M_{\odot}$ star would maintain a convective core at the TO even in the absence of overshooting. The chosen treatment and tuning of $\zeta$, then, does not substantially modify the occurrences at the TO for solar-type stars. Different would have been the case with instantaneous overshooting $\nu = 0.2$ (Fig. 7, dashed line), since the TO morphology in the whole range $1.0 \div 1.4M_{\odot}$ would have been substantially modified.

At the upper extreme of masses considered here, we see instead (Figs. 3 and 4) that diffusive overshooting with $\zeta = 0.02$ is, for a $15M_{\odot}$ star, nearly equivalent to instantaneous overshooting with $\nu = 0.2$, both for the HR diagram morphology, and for its effect of prolongating the MS lifetime (by about 15%). More in general, comparing Figs. 5 and 6 one can see that the effect of diffusive overshooting increases with the stellar mass in the range 1.5–2.0$M_{\odot}$, and finally becomes comparable with that of instantaneous overshooting with $\nu \sim 0.2$. So, working with diffusive mixing, a single value of $\zeta$ seems to be consistent with all the range of masses considered. In fact, it gives zero "equivalent" instantaneous overshooting for the solar mass, a

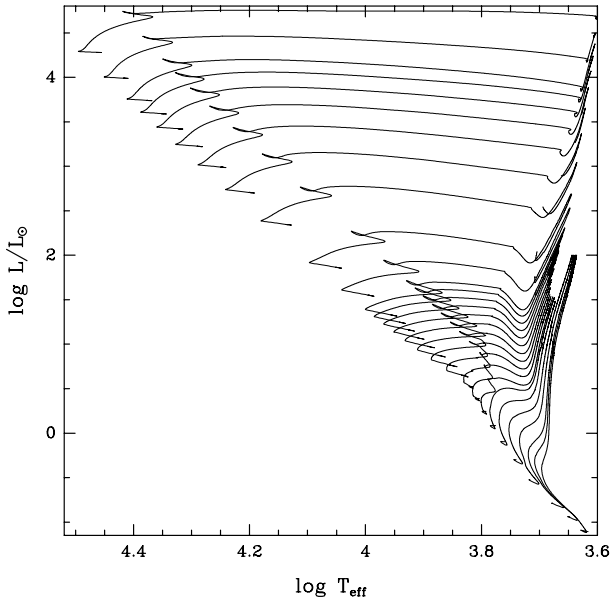


**Fig. 6.** HR diagram with diffusive overshooting, $\zeta = 0.02$

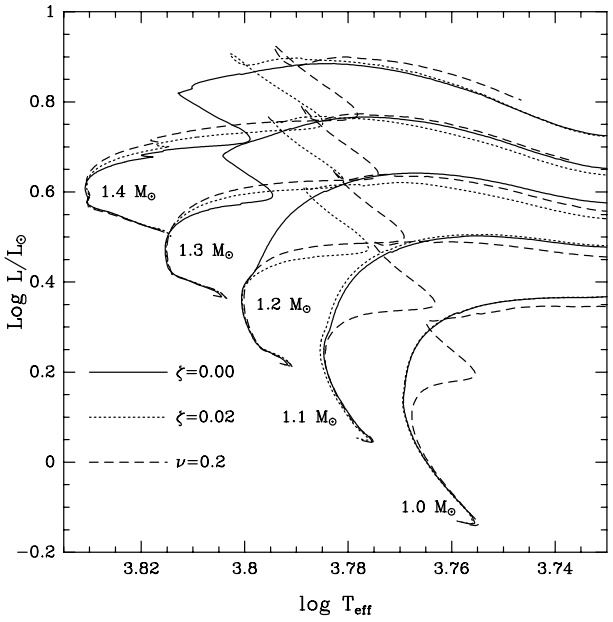


**Fig. 7.** Blow-up of the theoretical HR diagram for stars in the range $1.1 \div 1.3 M_{\odot}$, with and without diffusive overshooting. The difference between the two cases is that, with $\zeta = 0.02$, also the star of $1.2 M_{\odot}$ maintains a small convective core at the turn-off, while in the former case the same occurrence was found for $1.3 M_{\odot}$

slowly increasing effect for larger masses up to $\sim 2 M_{\odot}$, after which it mimicks $\sim 0.2 H_p$ of instantaneous overshooting.

The reason for this smooth growth of "equivalent" overshooting is mainly in the *non-local* flavor introduced in the models thanks to $f_{thick}$ in Eq. (4). As already quoted in Sect. 4.2, for low mass stars like the Sun the size of the initial convective core is quite small, much less than the value of $H_p$ at the convective boundary, and also the value of $f_{thick}$ is correspondingly low. This gives rise to a stiff velocity profile in the overshooting region, which in turn leads to very little mixing and fast fading of the core. For larger masses, the size of the core grows and so also $f_{thick}$, until saturation or quite so. Including some non-locality, even in a rough approximation, in the modeling of turbulent convection always gives more straightforward and physically realistic results, as already found for the superadiabatic temperature gradient thanks to the introduction of $z$ as convective scale length (Sect. 2.1). In the present case, we do not have to select different mass ranges with different tunings of the instantaneous overshooting parameter $\nu$; we can simply apply the same tuning for $\zeta$ to any mass range as a first, reasonable approximation.

## 6. Comparisons with previous evolutionary tracks

Among the several authors having provided in the past evolutionary sets of intermediate mass stars, the more recent ones are Chin & Stothers 1990, 1991; Schaller et al. (1992), Brocato & Castellani (1993), Schaerer et al. (1993), Mowlavi et al. (1994), Deng et al. (1996a,b). It is worth comparing our results with previous models computed with analogously updated micro-physical inputs, although an FST coupled-diffusive mixing and overshooting has not yet used by other authors. We then excluded from our comparisons the models by Chin & Stothers (1990, 1991) and by Brocato & Castellani (1993), since they adopted radiative opacities quite different from the updated OPAL ones present in our models. More reasonable are the comparisons with the results by Schaller et al. (1992, hereafter SSMM), Mowlavi & Forestini (1994, hereafter MF), Deng et al. (1996a,b,, hereafter DBC), since their input micro-physic is much closer to the one in **ATON 2.0** code. Of course, all the above quoted authors used the Mixing Length Theory (even if DBC worked out some corrections to the plain MLT) to deal with convection. In Fig. 8 we show the variation with mass of the hydrogen burning times computed by ourselves and by the authors mentioned above.

Before performing more detailed comparisons, we evaluated first–approximation transformations of luminosity and $T_{\rm eff}$ to slightly different chemistries, to better compare our results to the ones obtained in Zero Age Main Sequence (ZAMS) with different $(Y, Z)$ values. They turned out:

$$\delta \log L/L_{\odot} \simeq 1.79 \delta Y - 3.83 \delta Z$$

$$\delta \log T_{\rm eff} \simeq 0.42 \delta Y - 2.57 \delta Z$$

First we considered the models by SSMM, for ($Y$, $Z$)=(0.30, 0.020), in which instantaneous overshooting of $0.2 H_p$ is present. Given the chemistries, we must add to their ZAMS points the values $\delta \log L/L_{\odot} \simeq -0.035$ and $\delta \log T_{\rm eff} \simeq -0.0032$. The Zero Age Main Sequence locations turn out very similar; our ZAMS structures are in the average slightly more luminous and hotter, the maximum differences being however only $\sim .05$ in $\log L/L_{\odot}$ and $\sim 0.015$ in $\log T_{\rm eff}$. This similiarity is not surprising, since the physical inputs are very close both in SSMM and in our models.

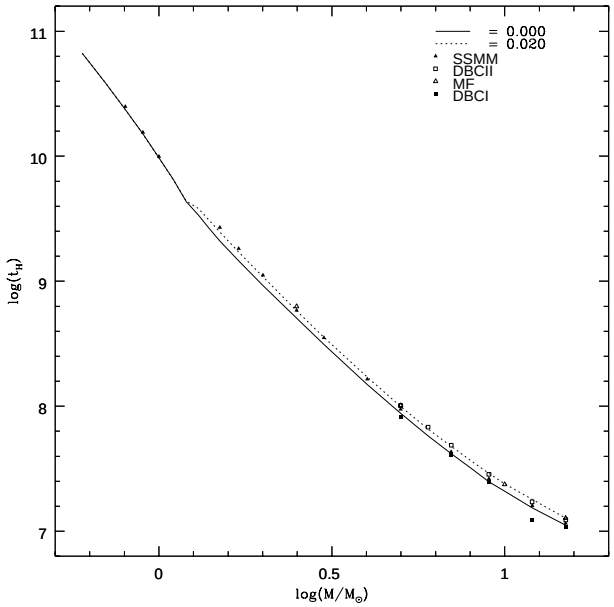


**Fig. 8.** Comparison of our results with those of other authors

This is not yet, however, a test on overshooting, which only affects the width of the MS. For the range of mass $1.5 \div 5 M_{\odot}$, also the width is similar in the present models with diffusive overshooting ($\zeta = 0.02$) and in SSMM. The average discrepancy is again of $0.01 \div 0.02$ in $\log T_{\rm eff}$. For larger masses ($7 \div 15 M_{\odot}$) the width of our MS band is slightly, sistematically larger ($0.04 \div 0.05$ in $\log T_{\rm eff}$). Closely related to the amplitude of MS is also its duration. In Fig. 8 we see that the lifetimes of stars in core $H$-burning phase in SSMM models are very similar to ours up to $\sim 4 M_{\odot}$, while SSMM get faster $H$-exhaustion for larger masses. At $15 M_{\odot}$, our lifetime in MS is $\sim 9\%$ longer than for SSMM. As already seen, half of the difference is due to our coupled-diffusion (Sect. 4.1) evolutionary scheme; the remaining $4 \div 5\%$ can be attributed to the non exact identity of diffusive and instantaneous overshooting, and to residual differences in the physical and chemical inputs between the two sets of models.

Analogous results are found when comparing our models with those by MF, where instantaneous mixing and overshooting with $\nu$ =0.20 are applied to models with $M$ =2.5, 5, 10, 15 $M_{\odot}$, and (Y, Z)=(.275,.020). Small differences in lifetime of H-burning ($2 \div 5\%$) are found; the width of our MS is slightly smaller than in MF by $0.002 \div 0.007$ (that is: almost negligible) in $\log T_{\rm eff}$ for the whole range of masses considered. Also the MS lifetimes are very close in both cases.

Interesting comparison can be made also with the DBC models, since they adopt a diffusive algorithm to deal with overshooting. For completeness, in Fig. 8 we also plot their models obtained with a classical instantaneous mixing scheme. The most outstanding result when comparing models obtained with diffusive overshooting is the similarity between our times of hydrogen burning with theirs over the whole range of masses spanned, our lifetimes being larger than their at $15 M_{\odot}$ just by $3 \div 4\%$, that is: the difference due to coupled-diffusion evolutionary scheme. We conclude then that, apart for this latter feature, the two overshooting algorithms used by DBC and by ourselves have almost the same effect, at least when dealing with main sequence stars of intermediate mass.

In the end, we want to stress what we already claimed, that is:

-this first test confirms that, on quantitative grounds, diffusive overshooting with $\zeta = 0.02$ gives results consistent with those obtained with instantaneous overshooting, $\nu = 0.2$, without having to care of setting overshooting to zero at $M < 1.5 \div 2.0 M_{\odot}$ and having a more physically sound description of the occurrences at the convective boundaries;

-the differences due to the use of the coupled-diffusion scheme instead of the instantaneous mixing one are of the same magnitude of other differences due to physical and chemical inputs; they must be accounted for in updated generations of stellar models.

**Table 4.** Lifetime H-burning (in unit of $10^6$ yr) DBC1 stands for classical mixing, while DBC2 for diffusive process

| $\frac{M}{M_{\odot}}$ | $t_H(noov)$ | $t_H(ov)$ | $t_H(PI)$ | $t_H(MF)$ | $t_H(DBC1)$ | $t_H(DBC2)$ |
|---|---|---|---|---|---|---|
| 0.6 | 66630.0 | 66651.5 | - | - | - | - |
| 0.65 | 50498.7 | 50512.6 | - | - | - | - |
| 0.7 | 38598.5 | 38623.4 | - | - | - | - |
| 0.8 | 23683.2 | 23684.3 | 25027.9 | - | - | - |
| 0.9 | 15079.6 | 15045.6 | 15500.3 | - | - | - |
| 1.0 | 9728.1 | 9685.2 | 9961.7 | - | - | - |
| 1.1 | 6517.3 | 6496.2 | - | - | - | - |
| 1.2 | 4343.3 | 4388.8 | - | - | - | - |
| 1.3 | 3381.5 | 3817.4 | - | - | - | - |
| 1.4 | 2623.3 | 3055.9 | - | - | - | - |
| 1.5 | 2097.0 | 2468.2 | 2694.7 | - | - | - |
| 1.7 | 1455.7 | 1713.8 | 1827.3 | - | - | - |
| 2.0 | 925.03 | 1086.1 | 1115.9 | - | - | - |
| 2.5 | 506.92 | 580.79 | 584.92 | 628 | - | - |
| 3.0 | 312.33 | 355.43 | 352.50 | - | - | - |
| 4.0 | 149.35 | 170.96 | 164.73 | - | - | - |
| 5.0 | 87.620 | 99.849 | 94.459 | 101.6 | 81.58 | 101.27 |
| 6.0 | 57.925 | 65.961 | - | - | - | 67.99 |
| 7.0 | 41.727 | 47.825 | 43.188 | - | 40.42 | 48.72 |
| 8.0 | 31.851 | 36.453 | - | - | - | - |
| 9.0 | 24.832 | 29.029 | 26.389 | - | 24.93 | 28.55 |
| 10.0 | 20.863 | 23.959 | - | 23.67 | - | - |
| 12.0 | 15.386 | 17.989 | 16.018 | - | 12.21 | 17.17 |
| 15.0 | 11.177 | 12.758 | 11.584 | 12.74 | 10.90 | 12.31 |

## 7. Isochrones and the age of young open clusters

We have computed isochrones from our models and have transformed them into the observational $M_v$–$B-V$ plane. The tracks are transformed by adopting Kurucz & Castelli (1996, private communication) model atmosphere relations between $T_{\rm eff}$ and $B-V$. The semiempirical transformations by Flower (1996) are similar, but provide bluer main sequence colors -by $\sim 0.05$ mag

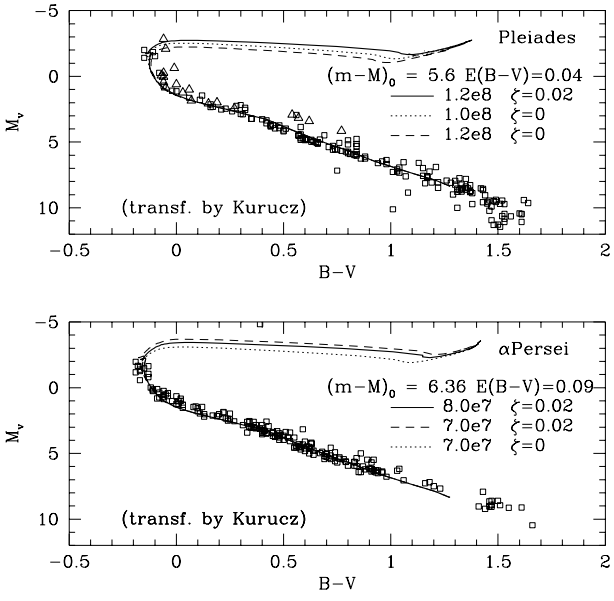


**Fig. 9.** Top figure: the Pleiades HR diagram data are taken from Iriarte (1969) photoelectric data (open triangles), and from a list by Stauffer 1984 and reference therein, (open squares). Stauffer's data are shown for the stars in common between the two lists. Superimposed we show the isochrone of $1.2\times10^8$ yr with diffusive overshooting (full line) and the isochrones of $10^8$ and $1.2\times10^8$ yr without overshooting. Although the turn-off region is scarcely defined by only six stars, the isochrone with overshooting provides a reasonable fit of the data, although the corresponding one without overshooting can not be excluded. Distance modulus and reddening are the pre-Hipparcos values. An age $\sim 15\%$ larger is obtained by assuming the Hipparcos distance modulus [$(m-M)_0 = 5.33$] but reducing the reddening to 0.02mag. In the bottom figure, the $\alpha$ Persei diagram is compared with our isochrones including overshooting for ages of 70 and 80Myr, and with the isochrone of 70Myr with no overshooting

– at $B-V \sim 0.5$, while the main sequence colors become definitely too red at $B-V \sim 1.5$.

Detailed comparisons with data in the literature will be postponed to a subsequent work. Current open problems of datation demand a preliminary application of the computed isochrones to the Pleiades cluster. There are in fact some recent problems regarding this cluster. First of all, the Hipparcos parallaxes have revised its distance modulus to $(m-M)_0 = 5.33$ from the previously accepted value of $(m-M)_0 = 5.6$ and this revision opens problems of compatibility with the other open clusters main sequences (Mermilliod et al. 1997). We will show here the comparisons made with the "classic" distance modulus $(m-M)_0 = 5.6$, with a reddening $E(B-V) = 0.04$ (e.g. Meynet et al. 1993). If we reduce the distance modulus to the Hipparcos value but at the same time bring down the reddening to the still acceptable value of 0.02, the main sequence location is still accurately reproduced (in this case, the agreement is better if we adopt Flower (1996) semiempirical correlations and the age is increased by 15% with respect to the present fit.

Second, the Pleiades have received a recent datation based on the luminosity location of the transition between stars without lithium in ther spectrum (HHJ3) and showing lithium (the candidate brown dwarf PPL 15). This age is $\sim 1.2\times10^8 yr$ (Basri et al. 1996), noticeably larger than what generally inferred for this cluster. Although the first datations of the Pleiades gave an age of $\sim 0.7\times10^8 yr$, more recent values (e.g. Meynet et al. 1993 models with overshooting) provided an age of $\sim 10^8 yr$, closer, but not yet fully consistent with the brown dwarf dating. Actually, Basri et al. (1996) datation could result to be a *lower limit*, as PPL15 is a binary, so it could not be an optimum marker for the luminosity at which lithium reappears.

We show in Fig. 9 the HR diagram of the Pleiades and our isochrones with and without overshooting. The continuous line is the isochrone of $1.2\times10^8 yr$ including overshooting, while the two dashed lines are the isochrones of $10^8$ and $1.2\times10^8 yr$ without overshooting. Noticeably, the isochrone with overshooting very reasonably fits the stellar locus, and its age is compatible with the result from the brown dwarfs observations. The age derived by Meynet et al. (1993), also on the basis of models including overshooting, is $10^8$ yr: as we have discussed above, the differences in the nuclear evolutionary scheme and in the chemistry (they adopt a larger helium content $Y = 0.30$ and metallicity $Z = 0.02$) provide somewhat shorter evolutionary times in the mass range which defines the Pleiades turnoff. The uncertainty on the age is in any case considerable: if we define the turnoff by requiring the full inclusion of the most luminous star, the age is smaller also in the models with overshooting. Neverthless, it is important that consistency between the brown dwarf dating and the turnoff dating is obtained. Given that the brown dwarf should provide more precise information than the turnoff datation (Basri 1997, D'Antona & Mazzitelli 1997, Bildsten et al. 1997), we regard this result as an indication that the models with overshooting are to be preferred to the standard models.

We also show in Fig. 9 the turnoff fitting of the cluster $\alpha$ Persei. Meynet et al. (1993) provide an age of 50 Myr, based on the fit of both the turnoff and of the subgiant star $\alpha$Per itself, interpreted as a star belonging to the blue loop of post-helium ignition evolution. Limiting ourselves to the turnoff, the resulting age can be as large as 80 Myr in our models with overshooting, but probably smaller than 70 Myr in the models without overshooting. Observations of Lithium in the brown dwarf candidates belonging to this cluster will provide another interesting constraints on the turnoff models.

## 8. Conclusions

We have updated both micro and macro-physical inputs in **ATON 2.0** code for general stellar evolution. In particular, we treated convective mixing inside and outside formally convective regions as a diffusive process.

Since the diffusion coefficients cannot yet be evaluated according to first principles, we assumed an FST local model to get the turbulent velocities (projected at the boundaries) inside formally convective regions, and exponential decay of the turbulent velocity outside. Elements of "non-locality" are introduced when considering the diffusive scale lengths tied to radial dis-

tances from convective boundaries. Full coupling between nuclear chemical evolution and turbulent mixing is assumed.

One relevant result is that the CNO equilibria in the convective cores of large mass main sequence stars do require such coupling in the models computation. Instantaneous or diffusive mixing decoupled from nuclear evolution leads to discrepances in the evaluation of evolutionary times.

As for overshooting, we chose a conservative value for the free parameter of diffusion $\zeta$ such that it should have a negligible effect on the early convective core of the Sun, and mimick the effect of an instantaneous overshooting of $\sim 0.20 H_p$ for intermediate to large mass stars. This tuning is obviously preliminary, and requires further tests and comparisons not only in main sequence but also in other evolutionary phases. Next papers on the subject will follow, with application of the present diffusive scheme mainly to horizontal branch and to thermally pulsating stars.

We also compared our results with the more recent ones in the literature, finding satisfactory agreement so far as the different chemical compositions and mixing schemes could allow.

## 9. Appendix: the ATON 2.0 code

### *9.1. Generalities*

In this appendix, we provide a synthetic but exhaustive description of the numerical inputs of the code **ATON 2.0**, to complement the elucidation in Sects. 2 and 3 of the main macro/micro-physical inputs. The choice of fully document the code will also help us, in the future, to avoid useless debates about results obtained from codes having different and/or not fully documented inputs.

**ATON 2.0** describes spherically symmetric structures in hydrostatic equilibrium. It has been conceived to follow the evolution of stellar objects from early pre-main sequence phases prior to D-ignition, down to final brown or white dwarf cooling (apart from dynamical phases like full degenerate He-ignition) or to the onset and early developement of $^{12}\mathrm{C}+^{12}\mathrm{C}$ reactions. The ignition of $^{16}\mathrm{O}+^{16}\mathrm{O}$ and the following (pre-supernova) phases are not accounted for. In future papers, we will always refer to an **ATON N.M** version of the code, where **N** will keep track of the major macro-physical updates (e.g. rotation, non grey atmospheres etc), and **M** of the micro-physical ones (thermodynamics, opacities etc). In the same spirit above discussed, any change of release will be fully documented.

### *9.2. The numerical structure*

The internal structure is integrated via the usual Newton–Raphson relaxation (Henyey) method, from the center to the base of the optical atmosphere ($\tau = 2/3$). The independent variable is the mass; the dependent ones are: 1) radius, 2) total luminosity, 3) total pressure and 4) temperature. To avoid numerical precision problems close to the surface, where $\Delta \mathrm{M}/\mathrm{M_{tot}}$ can be $\sim 10^{-12} \div 10^{-18}$, the code rezones and performs numerical derivatives directly on the $\Delta \mathrm{M}$ vector, and the local value of mass at each grid point is obtained as a summation of $\Delta \mathrm{M}$ from the center. This procedure, as opposed to the traditional one of computing grids of subatmospheres – with pressure as independent variable – down to a given fraction of $\mathrm{M_{tot}}$, allows straightforward evaluation of the gravothermal energy generation rate up to the stellar surface, especially when mass loss (e.g. in contact binaries) plays a dominant role on the structure.

Given the $\mathrm{i^{th}}$ grid point, and the $\mathrm{j^{th}}$ dependent variable $\mathrm{q_j(i)}$, the corrections $\delta \mathrm{q_j(i)}$ can be found from the solution of the system (in Einstein notation):

$$\frac{\partial EQ(1 \div 4)}{\partial q_j(i)} \delta q_j(i) + \frac{\partial EQ(1 \div 4)}{\partial q_j(i+1)} \delta q_j(i+1) + \beta(1 \div 4) = 0\,, \tag{A.1}$$

where $\mathrm{Eqs.}\ (1 \div 4)$ are the four canonical differential equations, and $\beta(1 \div 4)$ are the residuals. Since only two boundary conditions are known at the center, the values of $\delta \mathrm{q_j(i)}$ cannot be found until the surface is reached. We then compute at each grid point the matrix elements $\mu$ and $\nu$, and the vector elements $\epsilon$ such that

$$\delta q_j(i) = \mu_j^k(i) \delta q_k(i) + \nu_j^k(i) \delta q_k(i+1) + \epsilon_j(i) \tag{A.2}$$

The only non-vanishing coefficients are:

$\mu_1^3$; $\mu_1^4$; $\mu_2^3$; $\mu_2^4$; $\nu_3^3$; $\nu_3^4$; $\nu_4^3$; $\nu_4^4$; $\epsilon_j$

Once reached the surface (base of the optical atmosphere) the system is closed by the integration of three optical atmospheres, with (L,R), (L+$\delta$L,R), (L,R+$\delta$R). Backward application of Eq. (A2) allows the evaluation of all the $\delta \mathrm{q_j(i)}$'s. Note that, with the above choice, $\nu_3^3$ and $\nu_4^4 \sim 1$, and also all the other coefficients do not depart from unity for too many orders of magnitude, avoiding round-off and truncation errors. Also, during the iterations to convergency, the $\Delta \mathrm{q_j}$ values are updated as

$$\Delta q_{j(new)}(i) = \Delta q_{j(old)}(i) + \delta q_j(i+1) - \delta q_j(i)$$

and new values of $\Delta \mathrm{q_j}$ are differentially computed only after convergency.

### *9.3. Internal zoning, time steps and nuclear evolution*

Internal zoning of the structure is reassessed at each physical timestep, with particular care in the central and surface regions, in the vicinities of convective boundaries and H or He-burning shells, and close to the superadiabaticity peak. Tipically, pre-main sequence and main sequence structures are resolved in $800 \div 1200$ grid points; red giants in $1200 \div 1500$ grid points, $\sim 400$ of which in the thin H-burning shell; horizontal branch structures contain $1500 \div 2000$ grid points and, during thermal pulses, up to $\sim 3000$ grid points are often reached.

The physical time step is evaluated according to experience, allowing maximum variations, both integral and local along the structure, of several physical and chemical quantities. Among the integral quantities, total, CNO, $3\alpha$ and $^{12}\mathrm{C}+^{12}\mathrm{C}$ luminosities are considered; among the local ones, the four structural quantities and the central chemical compositions. The final time step chosen is obviously the shortest one out of the $\sim$

fifteen evaluated. For a solar-like star, evolution from pre-main sequence to turn-off takes $\sim 1000$ physical time steps; He-flash is reached after $15000 \div 20000$ time steps (no shell projection), in horizontal branch central He-exhaustion is reached in $\sim 2000 \div 4000$ time steps, and one fully developed thermal pulse cycle, from peak to peak takes $\sim 3000 \div 5000$ time steps.

So far we spoke of "physical" time steps. For the purposes of chemical evolution only, each physical time step is further divided into at least 10 "chemical" time steps. Any mechanism leading to a variation of chemical composition, such as nuclear evolution, gravitational settling and convective mixing, is repeatedly applied for the number of chemical time steps up to the reaching of the physical time step, projecting pressure and temperature to get also projected nuclear reaction rates. In this way, the evolution up to the He-flash can require up to $2 \times 10^5$ chemical time steps, and the advancement of an H-burning shell from step to step is only a tiny fraction of its thickness.

As for the chemical evolution, we adopt the implicit scheme by Arnett & Truran (1969). It can be assumed equivalent to a first order Runge-Kutta, since it accounts for both the initial and the final chemical composition in the evaluation of the reaction rates. The integration error is then proportional to $(\Delta X)^2$. The alternative approach to compute the rates for the initial abundances only can be instead assimilated to a zero order Runge-Kutta, and the integration error would be proportional to $(\Delta X)$, being then much larger. To restore better integration precision in this latter case, it is customary to divide each *physical* timestep in a large number of *chemical* timesteps, decreasing in this way $(\Delta X)$ for each step. Also in code **ATON 2.0**, however, the physical timestep is divided in several chemical ones, as above mentioned, leading to almost vanishing numerical errors in the nuclear evolution integration.

If instantaneous mixing of convective regions is adopted (not recommended, since diffusive mixing is more physically sound), the average chemistry and reaction rates over all the region are evaluated, and the linearization procedure applied to the whole region as a single grid point. The very small variations of chemistry with time obtained in this way ensure enormously better numerical precision of integration than the alternative procedure of locally evaluating the new chemistries and then mixing.

### *9.4. Diffusive mixing*

In the case of diffusive mixing, we must solve Eq. (1) to get the new chemical abundances $Y_{a,i}^{n+1}$ at time $t^{n+1}$ for each element $a$ at each mesh point $i$. Nuclear evolution and mixing are strictly interwined, so that their simultaneous resolution is invoked. We adopted a network of 22 nuclear reactions for 14 elements (Sect. 3.3).

The equation describing the rate of change of abundance for the nucleus $a$, having number density $N_a$, is:

$$\frac{\partial Y_a}{\partial t} = \frac{1}{r^2\rho}\frac{\partial}{\partial r}\left(r^2 \rho D \frac{\partial a}{\partial r}\right) \pm \sum_{l \geq k} Y_l Y_k \, [lk]$$

where $Y_a = N_a/\rho N_A$ ($N_A$ = Avogadro's number).

Using a finite difference method based on a two-time level and three-point scheme, Eq. (A1) can be approximated by

$$\begin{aligned} & A_a Y_{a,i}^{n+1} \\ & = A_a Y_{a,i}^{n} + \Delta t \Bigg\{ \sum [p,q]^{n+1/2} \\ & \times [Y_{p,i}^n Y_{q,i}^n + (Y_{p,i}^{n+1} - Y_{p,i}^n) Y_{q,i}^n + (Y_{q,i}^{n+1} - Y_{q,i}^n) Y_{p,i}^n] \\ & - \sum [a,j]^{n+1/2} [Y_{a,i}^n Y_{j,i}^n + (Y_{a,i}^{n+1} - Y_{j,i}^n) Y_{j,i}^n \qquad \text{(A2.a)} \\ & + (Y_{j,i}^{n+1} - Y_{a,i}^n) Y_{a,i}^n] + \frac{2A_a}{m_{i+1} - m_{i-1}} \\ & \times \left[ \sigma_{i+1/2}^{n+1/2} \frac{Y_{a,i+1}^{n+1} - Y_{a,i}^{n+1}}{m_{i+1} - m_i} - \sigma_{i-1/2}^{n+1/2} \frac{Y_{a,i+1}^{n+1} - Y_{a,i-1}^{n+1}}{m_i - m_{i-1}} \right] \Bigg\} \end{aligned}$$

$$Y_{a,base}^{n+1} = Y_{a,base+1} \qquad \text{(A2.b)}$$

$$Y_{a,surf}^{n+1} = Y_{a,surf-1} \qquad \text{(A2.c)}$$

where $\sigma_{i\pm1/2}^{n+1} = 16\pi^2 r^4 \rho^2 D$ is computed at half-integer grid points. The boundary conditions have the meaning of no convective flux at the boundaries of convective (plus overshooting – if any) region, since no mass exchange with the non turbulent regions of the star is allowed.

Equation (A2.a) can be rewritten as

$$\begin{aligned} & \Delta t \cdot B(a)_j = -\alpha_{a,i}\gamma_i Y_{a,i-1}^{n+1} - \alpha_{a,i}\beta_i Y_{a,i+1}^{n+1} \\ & + \Delta t \cdot \sum_k A(a,k)_i Y_{k,i}^{n+1} + \alpha_{a,i}\left(\gamma_j + \beta_i\right) Y_{a,i}^{n+1} \qquad \text{(A3)} \end{aligned}$$

where $\alpha_{a,i} = \frac{2\Delta t A_a}{m_{i+1} - m_{i-1}}$; $\beta_i = \frac{\sigma_{i+1/2}^{n+1/2}}{m_{i+1} - m_i}$; $\gamma_i = \frac{\sigma_{i-1/2}^{n+1/2}}{m_i - m_{i-1}}$ where A(a,k) stands for the coefficients of the $Y_{k,i}^{n+1}$ terms and B(a) stands for terms relative to time step $t^n$. Note that the abundance of each element at a given grid point is coupled to the abundances of all the other elements at the same grid point, and to its own abundance at adjacent grid points. Since the two boundary conditions are met at the base and at the top of convection, the problem can not be explicitly solved until the whole convective region is addressed.

We now provide a description of the numerical method adopted to solve the system (A3, A2.a, A2.b).

For each convective region of $Tot$ grid points, we should in principle compute, store and invert a $(14{\cdot}Tot, 14{\cdot}Tot)$ matrix. A careful analysis of Eq. (A3) shows however that the storage of a $(42, 14{\cdot}Tot)$ matrix is sufficient, since only the matrix elements close to the diagonal are nonzero. Our problem has been reduced to solve a system $A \cdot y = B$, where $A = (42, 14 \cdot Tot)$, while $B = (14 \cdot Tot)$.

Were A a square matrix, it would be possible to save computer time by applying the usual L–U (lower-upper) triangular decomposition (Crout's algorithm) such that $L \cdot U = A$. Iteratively evaluating L and U, and recalling that

$A \cdot y = (L \cdot U) \cdot y = L \cdot (U \cdot y) = B$

one would get the vector x such that $L \cdot x = B$, and finally the vector y so that $U \cdot y = x$.

We adapted Crout's algorithm to our matrix. Being $a$ and $j$ two generic chemical elements and i the spatial grid point (from

the base of the convective region $i = i_{bot}$, to the top $i = i_{top}$) the algorithms used to determine L and U are as follows:

$$i = i_{bot}\ ;\ 1 \le a \le NEC$$

$$U(NEC+a,a,i) = A(NEC+a,a,i)$$

$$L(a,a,i+1) = A(a,a,i+1)/U(NEC+a,a,i)$$

$$i_{bot} \le i < i_{top}\ ;\ 1 \le a \le NEC$$

$$U(2NEC+a,a,i) = A(2NEC+a,a,i)$$

$$i_{bot} < i \le i_{top}-1\ ;\ 1 \le a < NEC; a+1 \le j \le NEC$$

$$U(2NEC+a,j,i) = -\sum_{j=a+1}^{NEC}\sum_{m=a}^{j-1} U(2NEC+a,m,i)L(NEC+m,j,i)$$

$$i_{bot} \le i < i_{top}\ ;\ 1 \le a \le NEC; 1 \le j \le a$$

$$U(NEC+a,j,i+1) = A(NEC+a,j,i+1) - \sum_{m=1}^{j-1} L(NEC+m,j,i+1)U(NEC+a,m,i+1) - \sum_{m=a}^{NEC} L(m,j,i+1)U(2NEC+a,m,i)$$

$$i_{bot} \le i < i_{top}\ ;\ 1 \le a \le NEC; a+1 \le j \le NEC$$

$$L\ (NEC+a,j,i+1) = \frac{A(NEC+a,j,i+1)}{U(NEC+a,a,i+1)} - \frac{\sum_{m=1}^{a-1} L(NEC+m,j,i+1)U(NEC+a,m,i+1)}{U(NEC+a,a,i+1)} - \frac{\sum_{m=j}^{NEC} L(m,j,i+1)U(2NEC+a,m,i)}{U(NEC+a,a,i+1)}$$

$$i_{bot} \le i < i_{top}-1\ ;\ 1 < a \le NEC; 1 \le j < a$$

$$L(a,j,i+2) = -\frac{\sum_{m=j}^{a-1} L(m,j,i+2)U(NEC+a,m,i+1)}{U(NEC+a,a,i+1)} \qquad \text{(A3)}$$

$$i_0 \le i < i_{surf}-1\ ;\ 1 \le a \le NEC$$

$$L(a,a,i+2) = \frac{A(a,a,i+2)}{U(NEC+a,a,i+1)}$$

Since the terms of the L and U matrices do not occupy the same location, and since each element of matrix A is used just once to evaluate the corrisponding ones of matrices L and U, these new elements can be stored in matrice A.

The iterative procedure to evaluate the vector x is:

$$i_{bot} < i \le i_{top}\ ;\ 1 \le a \le NEC$$

$$X(a,i) = B(a,i) - \sum_{m=a}^{NEC} A(m,a,i)X(m,i-1) - \sum_{m=1}^{a-1} A(NEC+m,a,i)Y(m,i)$$

Finally the new abundances $Y(a,i)$ for each element can be obtained from the following:

$$i = i_{top}\ ;\ a = NEC$$

$$Y(a,i) = \frac{X(a,i)}{A(2a,a,i)}$$

$$i = i_{top}\ ;\ NEC < a \le 1$$

$$Y(a,i) = \frac{\left[X(a,i) - \sum_{m=a+1}^{NEC} A(NEC+m,a,i)X(m,i)\right]}{A(NEC+a,a,i)}$$

$$i_{top} < i < i_{bot}\ ;\ NEC \le a \le 1$$

$$Y(a,i) = \frac{X(a,i)}{A(NEC+a,a,i)} - \frac{\sum_{m=1}^{a} A(2NEC+m,a,i)X(m,i+1)}{A(NEC+a,a,i)} - \frac{\sum_{m=a+1}^{NEC} A(NEC+m,a,i)X(m,i)}{A(NEC+a,a,i)}$$

$$i = i_{top}\ ;\ a = NEC$$

$$Y(a,i) = -\frac{A(2NEC+a,a,i)X(a,i+1)}{A(NEC+a,a,i)}$$

To further reduce storage allocation, it is again possible to store each new element Y(a,i) in the corrisponding location of X(a,i).

## References


Alcock C., Illarionov A. 1980, ApJ 235, 541
Alexander D.R., Ferguson J.W. 1994, ApJ 437, 879
Aller L.H., Chapman S. 1960, ApJ 132, 461
Arnett W.D., Truran J.W. 1969, ApJ 157, 359
Bahcall J.N., Pinsonneault M.H. 1992, Rev. Mod. Phys. 64, 885
Basri G. 1997 in "Cool Stars in Clusters ans Associations" eds. R. Pallavicini & G. Micela, Mem.S.A.It., 68, n.4
Basri G., Marcy G., Graham J.R. 1996, ApJ 458, 600
Basu S., Antia H.M., 1997, MNRAS 287, 189
Bildsten L., Brown E.F., Matzener C.D., Ushomirski G. 1997, ApJ 482, 442
Brocato E., Castellani V. 1993, ApJ 410, 99
Canuto V.M. 1992, ApJ 392, 218
Canuto V.M., Mazzitelli I. 1992, ApJ 389, 724
Canuto V.M., Goldman I., Mazzitelli I. 1996, ApJ 473, 550
Caughlan G.R., Fowler W.A. 1988, Atomic Data Nucl. Tab. 40, 283
Chin C.W., Stothers R.B. 1990, ApJS 73, 821
Chin C.W., Stothers R.B. 1991, ApJS 77, 299
Chiosi C. 1997, in "Stellar Astrophysics for the Local Group: a first step to the Universe", eds. A.J. Aparicio & A. Herrero, Cambridge University Press, in press

Christensen - Dalsgaard J., Gough D.O., Thompson M.J. 1991, ApJ, 378, 413
Cloutman L.D., Eoll J.G. 1976, ApJ 206, 548
D'Antona F., Mazzitelli I. 1997, in "Cool Stars in Clusters and Associations", eds. R. Pallavicini & G.Micela, Mem.S.A.It., 68, n.4
Deng L., Bressan A., Chiosi C. 1996a, A&A 313, 145
Deng L., Bressan A., Chiosi C. 1996b, A&A 313, 159
Flower P.J., 1996, ApJ, 469, 335
Fontaine G., Michaud G. 1979, in IAU Colloquium 53, *White dwarfs and variable degenerate stars*, ed. H. M. Van Horn and V. Weidemann (Rochester, N.Y.: University of Rochester), 192
Fontaine G., Graboske H.C. Jr., Van Horn H.M. 1977, ApJ Suppl. 35 n. 3, 293
Graboske H.C., De Witt H.E., Grossman A.S., Cooper M.S. 1973, ApJ 181, 457
Grevesse N., 1984, Phys. Scr., T8, 49
Grevesse N., Noels A. 1993, in *Origin and evolution of the Elements*, ed. N. Prantzos, E. Vangioni - Flam, and M. Cassé (Cambridge: Cambridge University Press), 14
Grossman S.A. 1996, MNRAS 279, 305
Iben I., MacDonald J. 1985, ApJ 296, 540
Iriarte A. 1969, Boll. Obs. Tonantzintla y Tacubaya 5, 89
Itoh N., Kohyama, Y. 1993, ApJ 404,268
Itoh N., Mutoh H., Hikita A., Kohyama Y. 1992, ApJ 395, 622
Lamb H., 1932, Hydrodynamics (Cambridge: Cambridge University press)
Kurucz R.L. 1993, CD-ROM 13 and CD-ROM 14
Maeder A. 1990, A&AS 84, 139
Maeder A., Meynet G. 1987, A&A 182, 243
Maeder A., Meynet G. 1991, A&AS 89, 451
Magni G., Mazzitelli I. 1979, A&A 72, 134
Mermilliod J.C., Turon C., Robichon N., Arenou F., Lebreton Y., 1997, in "Hipparcos Venice '97", ESA SP-402, p.643
Meynet G., Mermilliod J.C., Maeder A., 1993, A&AS 98, 477
Mihalas D., Dappen W., Hummer D.G. 1988, ApJ 331, 815
Mowlavi N., Forestini M. 1994, A&A 282, 843
Muchmore D. 1984, ApJ, 278, 769
Paquette C., Pelletier C., Fontaine G., Michaud G. 1986, ApJS 61, 1977
Prandtl L. 1925, Zs. Angew. Math. Mech. 5, 136
Profitt C.R., Michaud G. 1991, ApJ, 371, 584
Rogers F.J., Iglesias C.A. 1993, ApJ 412, 572
Rogers F.J., Swenson F.J., Iglesias C.A. 1996, ApJ 456, 902
Roxburgh W. 1978, A&A 65, 281
Sackmann J., Boothroyd A.I. 1995, Mem. Soc. Astr. It. 66, n.2, 403
Salasnich B., Bressan A., Chiosi C. 1997, A&A, submitted
Saumon D. 1994, in *The equation of state in Astrophysics*, ed. G. Chabrier and E. Shatzmann (Cambridge: Cambridge University Press), 306
Saumon D., Chabrier G., Van Horn H.M., 1995, ApJS 99, 713
Schaerer D., Meynet G., Maeder A., Schaller G. 1993, A&AS 98, 523
Schaller G., Schaerer D., Meynet G., Maeder A. 1992, A&AS 96, 269
Shaviv G., Salpeter E.E. 1973, ApJ 184, 191
Stauffer J. 1984, ApJ 280, 189
Stothers R.B., Chin C.W. 1992, ApJ 390, 136
Vitense E., 1953, Zs. Ap. 32, 135
Xiong D.R. 1985, A&A 150, 133